Physics of the Dark Universe 44 (2024) 101449

Contents lists available at ScienceDirect

Physics of the Dark Universe

journal homepage: www.elsevier.com/locate/dark

Full length article

# The excess of diffuse radio emission in galaxy clusters A4038 and A1664

Z.Z. Abidin [a], N. Asmi [a,*], M.R. Mat Sabri [a], M.A. Rohaizi [a], N. Hashim [b], U.F.S.U. Ibrahim [a]

[a] Department of Physics, Faculty of Science, University of Malaya, Kuala Lumpur, 50603, Malaysia
[b] Mathematics Division, Centre for Foundation Studies in Science, University of Malaya, Kuala Lumpur, 50603, Malaysia

ARTICLE INFO

*Keywords:*
Dark Matter
Indirect detection
Non-thermal radiation
Galaxy clusters
Cosmic ray

ABSTRACT

In this study, we investigate the potential connection between Dark matter (DM) particles and synchrotron emission in galaxy clusters, with a focus on radio relics. We explore three models beyond the standard model of particle physics and calculate emissions from DM particle candidates, comparing the results to radio observations. Our analysis centres on galaxy clusters A4038 and A1664, considering their radio properties and magnetic field characteristics. We employ the Navarro, Frenk, and White (NFW) profile to represent mass density distributions and in situ acceleration models for cosmic ray contributions. We estimate upper limits on DM cross-section annihilation $\langle \sigma v \rangle$ for various DM particle candidates for two decay channels ($b\bar{b}$ and $\mu^+\mu^-$ decay channels). Our findings suggest that the DM is not likely the source of the excess emission, but we acknowledge the potential impact of DM on total radio emissions in galaxy clusters. Further studies are needed to refine excess emissions and assess DM's influence on the total radio emissions. In summary, this research delves into the intricate relationship between DM particles and radio emissions in galaxy clusters, emphasizing the need for precise modelling and observation to unveil the mysteries of DM.

## 1. Introduction

According to the standard model of cosmology, the observable universe only accounts for approximately 5% of the total mass-energy content of our universe today. The remaining 95% is composed of substances that lie beyond the scope of our current knowledge and theories. A significant portion, about 69%, is attributed to dark energy, responsible for driving the accelerating expansion of our universe. The remaining 26% is dark matter (DM) [1], which serves as the focal point of investigation in this study.

In theory, if DM particles indeed exist, their self-annihilation can lead to the production of synchrotron emissions. These emissions arise from the interaction between the positron–electron pairs produced from DM self-annihilation and the magnetic field of a specific galaxy cluster, and they can be indirectly detected, as previously discussed by various authors [2–5].

Radio haloes are typically located in the central regions of galaxy clusters, while relics are predominantly found in the outskirts, near the peripheries of the clusters and towards the edges of the X-ray emissions [6]. Haloes typically exhibit a smoother, circular morphology, while relics tend to have elongated and arc-like shapes. The primary source of this radio continuum emission is the synchrotron radiation generated by relativistic electrons accelerated by shockwaves. The origin of these relativistic electrons may be linked to the theory of DM self-annihilation, as mentioned previously.

In addition to the relativistic electron abundances, numerous studies have reported excess emissions in various galaxy clusters [7–9]. We propose that the excess emission resulting from the decay of DM particles within the DM halo can account for this excess emission in our galaxy cluster samples, specifically A4038 and A1644. Table 1 displays the excess emission at different frequencies.

As shown in Table 2 of [10], it is necessary to subtract the contribution of discrete sources from the total emission of the observed area to isolate the radio relic emission. This is because discrete sources can be identified as compact radio sources. However, at frequencies of 0.029, 0.327, 0.408, and 0.843 GHz, the obtained radio relic emissions were not subtracted from the discrete sources. Instead, they were corrected using an extrapolation method introduced by [11]. The emissions were extrapolated and subsequently corrected to accommodate the contributions from discrete sources. This implies that the correction method validates the existence of discrete sources responsible for the excess emissions. Therefore, the excess emissions can be interpreted as the outcome of 1) Subtracting the total emission of the observed area from the radio relic emission and 2) the correction method. Currently, the excess emission for A4038 and A1664 is attributed to the discrete sources, whether they are unresolved sources or those identified through optical detection, as described in [10].

At the atomic scale, we delve into the realm of DM particle candidates that exist beyond the Standard Model of particle physics.

* Corresponding author.
*E-mail addresses:* zzaa@um.edu.my (Z.Z. Abidin), syzwniasmi@gmail.com (N. Asmi).

https://doi.org/10.1016/j.dark.2024.101449
Received 24 November 2023; Received in revised form 14 February 2024; Accepted 15 February 2024
Available online 20 February 2024

**Table 1**
The diffuse radio emission in A1644 (Top) and A4038 (Bottom).
*Source:* Data was taken from [10].

| A1664 | | | |
|---|---|---|---|
| $\nu$(GHz) | Radio relic emission (Jy) | Total emission of the observed area (Jy) | Excess emission (Jy) |
| 0.15 | 1.25 | 1.811 | 0.561 |
| 0.325 | 0.45 | 0.688 | 0.238 |
| 1.4 | 0.106 | 0.178 | 0.072 |
| **A4038** | | | |
| $\nu$(GHz) | Radio relic emission(Jy) | Total emission of the observed area (Jy) | Excess emission (Jy) |
| 0.029 | 32 | 42 | 10 |
| 0.074 | 12.45 | 12.6 | 0.15 |
| 0.150 | 5.16 | 5.26 | 0.1 |
| 0.240 | 2.96 | 3.04 | 0.08 |
| 0.327 | 1.4 | 1.54 | 0.14 |
| 0.408 | 0.91 | 0.96 | 0.05 |
| 0.606 | 0.38 | 0.427 | 0.047 |
| 0.843 | 0.17 | 0.21 | 0.04 |
| 1.4 | 0.06 | 0.086 | 0.026 |

**Table 2**
The radio properties of selected galaxy clusters.

| Name | redshift | radius (kpc) | $M_{vir}$ ($10^{14} M_{\odot}$) | $c_{vir}$ |
|---|---|---|---|---|
| A4038 | 0.0282 | 1000 | 9.62 | 12.46 |
| A1664 | 0.1280 | 1030 | 26.68 | 9.38 |

**Table 3**
The magnetic field properties of selected galaxy clusters.

| cluster | $\beta$ | $r_{core}$ (kpc) | $B_0$ (μG) | $\eta$ | $n_{gas}$ ($10^{-2}$ cm$^{-3}$) |
|---|---|---|---|---|---|
| A4038 | 0.541 | 43 | 6.6 | 0.5 | 1.74 |
| A1664 | 0.55 | 50 | 10 | 0.5 | 22.8 |

Numerous models have been developed to elucidate the nature of DM. In this paper, we concentrate on three models: the Minimum Universal Extra-Dimensional (MUED), the Simple Extension of the Standard Model (SIMP), and the Minimal Supersymmetric extension of the Standard Model (MSSM). Throughout this paper, we employ the symbol $\chi$ to represent all the respective DM particle candidates.

Our primary objective is to compute the emissions originating from these DM particle candidates. Additionally, we endeavour to quantify the emissions generated by cosmic ray particles. These emissions are then compared with the total emission of the area's observational data to perform likelihood tests and ascertain test statistic values. Employing the log–log fitting method, we derive the upper limit on the cross-section annihilation, denoted as $\langle \sigma v \rangle$.

## 2. Methodology

### 2.1. Sample selection

We restricted our galaxy cluster sample to those with redshifts ($z$) less than or equal to 0.13. In order to achieve more robust constraints, we favoured galaxy clusters with low observed diffuse radio emissions. Specifically, we selected galaxy clusters with prior reports of discrete radio sources. The chosen galaxy clusters are Abell 4038 (A4038) and Abell 1664 (A1664). We focused on these selected clusters to identify the concept of excess emission. Detailed radio properties for both clusters are provided in Table 2.

### 2.2. Density profiles and magnetic fields

Assuming that the DM halo has a spherical shape, we adopted the Navarro, Frenk, and White (NFW) profile, as described by Navarro et al. in 1997 [12], to represent the gravitational mass density distributions of the galaxy clusters under investigation. The NFW profile is defined as follows:

$$\rho(r) = \frac{\rho_s}{(r/r_s)(1 + r/r_s)^2} \tag{1}$$

The parameters $\rho_s$ and $r_s$ represent the characteristic density and scale radius of the NFW profile, respectively. These values can be determined based on the cluster's virial mass, denoted as $M_{vir}$, and its virial concentration, denoted as $c_{vir}$, which are sourced from the data provided in [13] and listed in Table 2. We employed COLOSSUS, a Python module [14], to compute the values of $\rho_s$ and $r_s$.

Assuming that DM is exclusively composed of a single particle at a time, chosen from the MUED, SIMP, and MSSM models, we can express the DM number density according to this equation:

$$N_{\chi}(r) = \frac{\rho(r)}{m_{\chi}} \tag{2}$$

Here, $\rho(r)$ is given by Eq. (1), and $m_{\chi}$ represents the mass of the DM particle.

The investigation of the cluster's magnetic field indicates that the magnetic field strength scales with the intracluster gas density, expressed as $B \propto n_{\rm gas}^{\eta}$, where $B$, $n_{\rm gas}$, and $\eta$ are the magnetic field strength, gas density, and proportional index, respectively, as detailed in [15]. We adopted the standard $\beta$ model for both the gas density profile and the magnetic field profile:

$$B(r) \propto n_{gas}(r)^{\eta} = B_0 (1 + \frac{r^2}{r_c^2})^{-(3/2)\beta\eta} \tag{3}$$

In the magnetic field profile, the parameters $B_0$, $r_c$, and $\beta$ represent the central magnetic field strength, core radius, and the $\beta$ parameter, respectively. Table 3 provides the necessary variables for calculating the magnetic field profile. It is worth noting that the values of $B_0$ and $\eta$ for A1664 were not available. Consequently, we employed assumptions derived from [16] for $B_0$ at the value of 10 μG, and from [17] for $\eta$ at 0.5.

The assumption of $B_0$ value is due to its cool core observation by [18] and uniform magnetic field distribution by [16]. While $\eta$ value relied on the correlation model between the magnetic field and the intra-cluster gas density in galaxy clusters. Our results are, therefore, inherently dependent on the validity of these assumptions.

### 2.3. Cosmic ray contribution

To account for the cosmic ray contribution in our analysis, we considered several models. Given our assumption that the radio relic emission is predominantly due to cosmic ray emission, we specifically employed the in situ acceleration models [19–21] to derive relevant

values. This model demonstrates the cosmic ray's role within our DM hypothesis. The in situ acceleration model is represented as:

$$S_{CR} = S_{CR,0}(\upsilon)^{-\alpha} \exp\left(\frac{-\upsilon^{1/2}}{\upsilon_s^{1/2}}\right) \tag{4}$$

In this equation, the parameters include the initial power-law contribution ($S_{CR,0}$), a uniform spectral index ($\alpha$), and a cutoff frequency ($\upsilon_s$), which are free parameters used for fitting, as described in [22].

A previous study [7] demonstrates that the in situ acceleration model fits well with the observations of A4038. However, no literature is available to confirm a good fit for A1664. Despite this, we have decided to use the in situ acceleration model as we are confident in its relevance to A1664. It is important to recognize, however, that the assumed cosmic ray spectrum may not entirely capture the features of the spectrum of A1664. We acknowledge the uncertainties associated with the cosmic ray spectrum and the possibility that employing an alternative model or form for the spectrum might yield different results in our analysis.

### 2.4. DM annihilations and synchrotron emission

We employed MadDM [23] to obtain the values of electron spectrum ($\frac{dN}{dE}$), $\langle\sigma v\rangle$ and the branching ratio (BR) for the individual annihilation channels. Additionally, we utilized the model from Feynrule [24] for all particle models, namely the MSSM, MUED, and SIMP.

For the MSSM model, we selected the particle neutralino (n1) as the DM candidate, as indicated in [25,26]. In the MUED model, we chose the photon Kaluza–Klein (a1) and weak Kaluza–Klein (z1) particles, as detailed in [27,28]. Lastly, for the SIMP model, we considered the real scalar DM (xd) and Dirac spinor DM (xr) as our DM candidates, as explained in [29,30].

After obtaining the values of $\frac{dN}{dE}$, $\langle\sigma v\rangle$ and the BR for each annihilation channel associated with these candidates, we calculated the electron source spectrum $Q_e(r, E)$ using the following equation [31–33]:

$$Q_e(r, E) = \sum_f \langle\sigma v\rangle \frac{dN}{dE}^f BR_f \frac{N_\chi(r)^2}{2} \tag{5}$$

In the equation, $f$ represents the annihilation channel, $\langle\sigma v\rangle$ denotes the cross-section for annihilation, and $N_\chi(r)$ represents the DM number density as defined in Eq. (2). To account for the contribution from positrons, the source spectra in all subsequent calculations will be multiplied by a factor of 2.

The source spectrum equation quantifies the number of electrons (N) with energy (E) resulting from the self-annihilation of DM particle models injected into the astrophysical environment. This spectrum is a fundamental aspect of our analysis.

Charged annihilation products are subject to acceleration by the magnetic fields within galaxy clusters. It is important to note that magnetic fields in galaxy clusters are not uniformly distributed but rather exhibit a tangled structure. Consequently, the evolution of electrons within the galaxy cluster can be mathematically described by the diffusion-loss equation:

$$\frac{\delta n_{eq}(r, E, t)}{\delta t} = \frac{\delta}{\delta E}[b(r, E) n_{eq}(r, E)] + Q_e(r, E) \tag{6}$$

In the equation, $n_{eq}(r, E, t)$ represents the electron equilibrium spectrum, and $b(r, E)$ denotes the energy loss due to synchrotron emission, inverse Compton scattering, Coulomb radiation, and bremsstrahlung radiation. The following four equations detail the expressions for each of these energy loss terms, measured in units of $GeV^{-1}$:

$$b_{syn}(B, E) = 2.53 \times 10^{-18} \left(\frac{E}{1\ \text{GeV}}\right)^2 \left(\frac{B}{1\ \mu\text{G}}\right)^2 \tag{7a}$$

$$b_{IC}(E) = 3.07 \times 10^{-17}(1+z)^4 \left(\frac{E}{1\ \text{GeV}}\right)^2 \tag{7b}$$

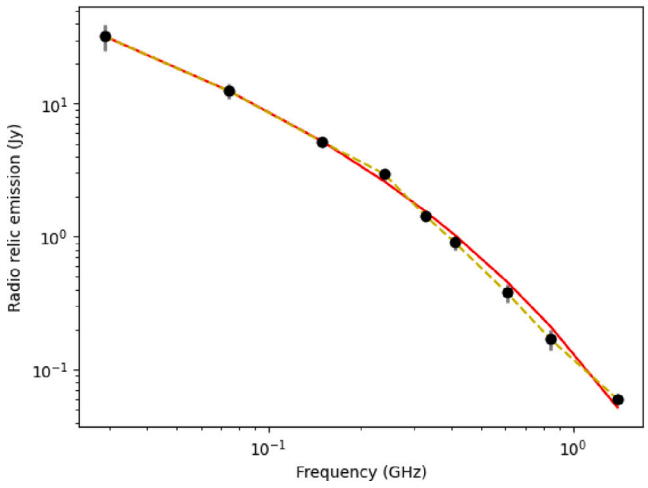


**Fig. 1.** The radio relic emission in A4038. The observational data is extracted from [10]. The red line represents the spectrum described by Eq. (4) with the best-fitting parameters: $S_{CR,0}$ = 9.76 Jy, $\alpha$ = 0.54, and $\upsilon_s$ = 0.055 GHz. The yellow dashed line represents the spectrum from the adiabatic compression model by [10]. (For interpretation of the references to colour in this figure legend, the reader is referred to the web version of this article.)

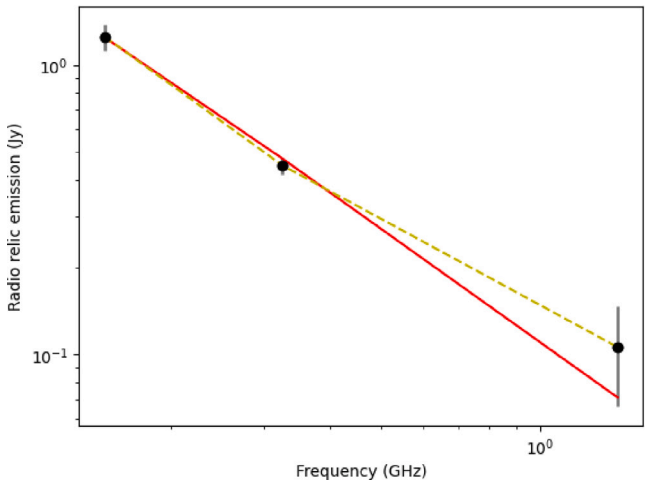


**Fig. 2.** The radio relic emission in A1664. The observational data is extracted from [10]. The red line represents the spectrum described by Eq. (4) with the best-fitting parameters: $S_{CR,0}$ = 0.15 Jy, $\alpha$ = 1.71, and $\upsilon_s$ = 10.5 GHz. The yellow dashed line represents the spectrum from the adiabatic compression model by [10]. (For interpretation of the references to colour in this figure legend, the reader is referred to the web version of this article.)

$$b_{Coul}(E) = 6.13 \times 10^{-16} n_{gas}(r) \left[1.0 + \frac{\ln(\gamma/n_{gas}(r))}{75}\right] \tag{7c}$$

$$b_{brem}(E) = 7.72 \times 10^{-20} n_{gas} \gamma [ln(\gamma) + 0.36] \tag{7d}$$

where $n_{gas}$ is in unit of $cm^{-3}$.

Electrons resulting from the annihilation of DM candidates are continually injected into the clusters. Over time, the electron spectra will reach a time-independent equilibrium state, which can be mathematically represented as the equilibrium spectrum $n_{eq}(r, E)$:

$$n_{eq}(r, E) = \frac{1}{b(r, E)} \int_E^\infty Q_e(r, E')\, dE' \tag{8}$$

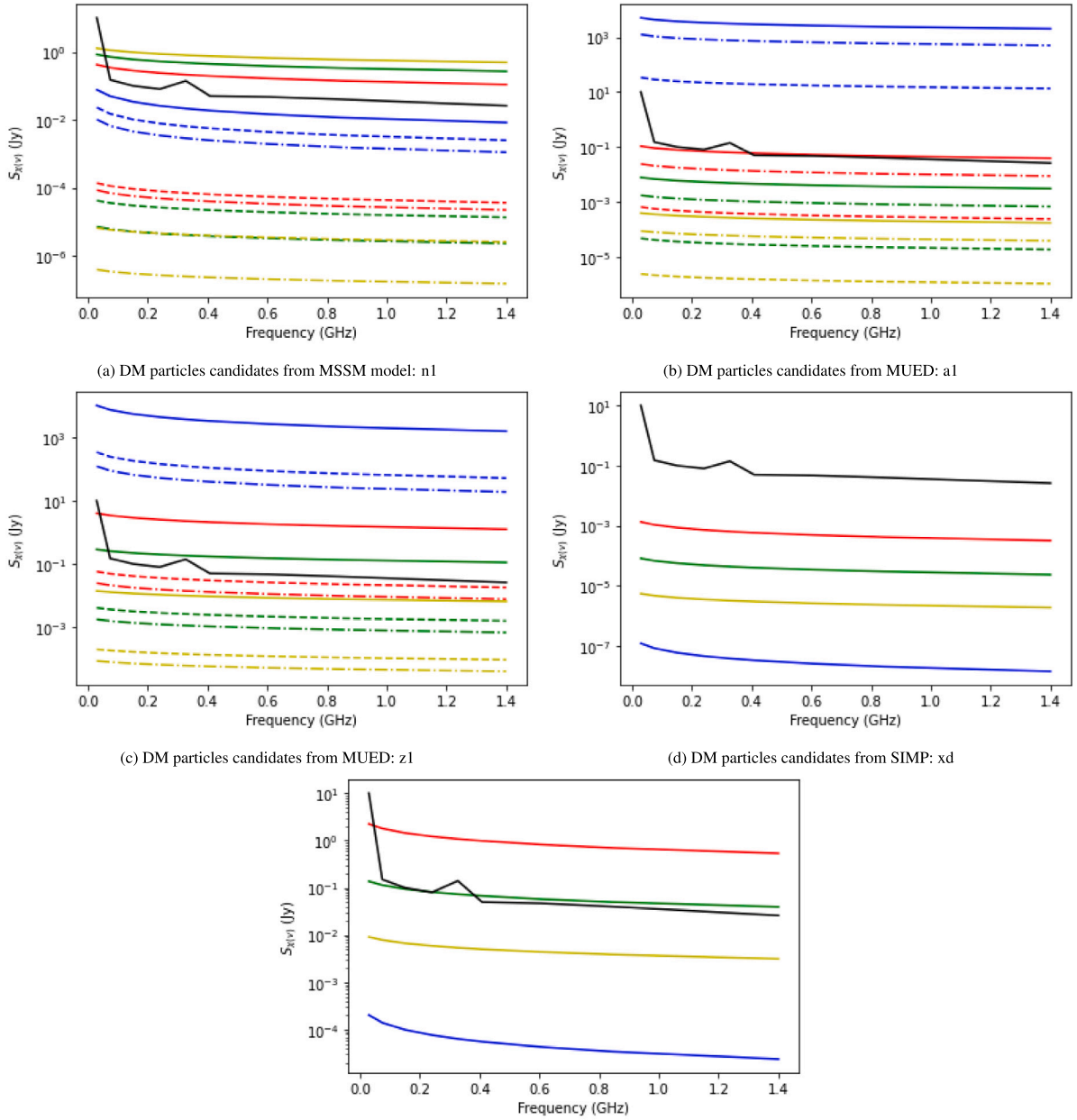


(a) DM particles candidates from MSSM model: n1

(b) DM particles candidates from MUED: a1

(c) DM particles candidates from MUED: z1

(d) DM particles candidates from SIMP: xd

(e) DM particles candidates from SIMP: xr

**Fig. 3.** The DM annihilation emission in A4038 as calculated using Eq. (11). The black line represents the excess emission from Table 1. Four selected DM masses are shown (n1, a1, z1: 40 GeV in blue, 850 GeV in red, 1750 GeV in green, and 4000 GeV in yellow; xd, xr: 130 GeV in blue, 940 GeV in red, 1840 GeV in green, and 4000 GeV in yellow). The solid line represents the all annihilation channel (aac), the dashed line represents the $b\bar{b}$ channel, and the dash-dot line represents the $\mu^+\mu^-$ channel. Note that xr and xd only have aac. (For interpretation of the references to colour in this figure legend, the reader is referred to the web version of this article.)

The synchrotron radiation emissivity of relativistic electrons per unit volume, resulting from the decay of DM self-annihilations, with kinetic energy in the range from $E$ to $E + dE$ and averaging over all pitch angles, is described by [34] as:

$$\epsilon_v(r) = \frac{\sqrt{3}e^3}{m_e c^2} \int_{E_{min}}^{E_{max}} n_{eq}(r, E) R(x) B(r)\, dE \tag{9}$$

where $R(x)$ is defined as (Ghisellini, Guilbert & Svensson 1988) [35]:

$$R(x) \equiv 2x^2 K_{4/3}(x) K_{1/3}(x) - \frac{3}{5} x [K^2_{4/3}(x) K^2_{1/3}(x)] \tag{10}$$

Here, the symbol $K$ represents the modified Bessel function, and $x = \frac{2\pi m_e^3 c^5 \nu}{3eBE^2}$, where $m_e$, $c$, and $\nu$ stand for the electron mass, speed of light, and photon frequency, respectively. The DM distribution is assumed to be spherically symmetric. To determine the total luminosity of the cluster, we integrated the radio powers over the radius from the cluster centre.

The synchrotron radio emission was then obtained by the equation:

$$S_{\chi(v)} = \frac{4\pi \int_0^R r^2 \epsilon_v(r)\, dr}{4\pi D_L^2} \tag{11}$$

where $D_L$ is the luminosity distance of the galaxy cluster.

In our subsequent sections, we will present the results and engage in discussions regarding the cosmic ray contribution, and the DM annihilation contribution, and explore the potential implications of DM contributions as they relate to the excess emission in observational data. Additionally, we will establish constraints on the DM mass and cross-section annihilation for each of the DM particle candidates.

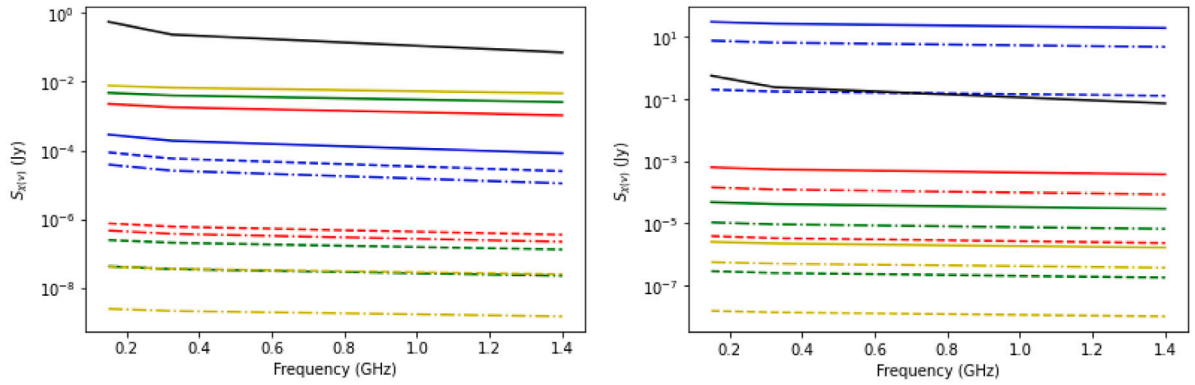


(a) DM particles candidates from MSSM model: n1




(b) DM particles candidates from MUED: a1

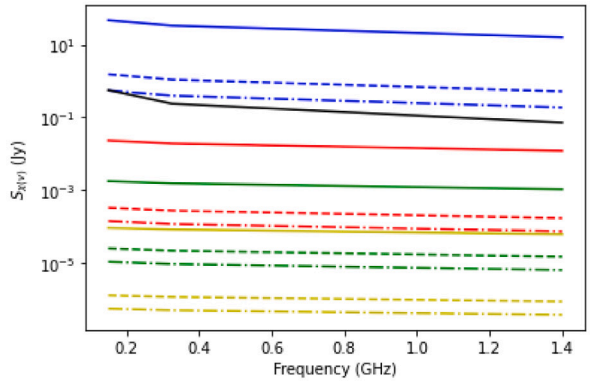


(c) DM particles candidates from MUED: z1

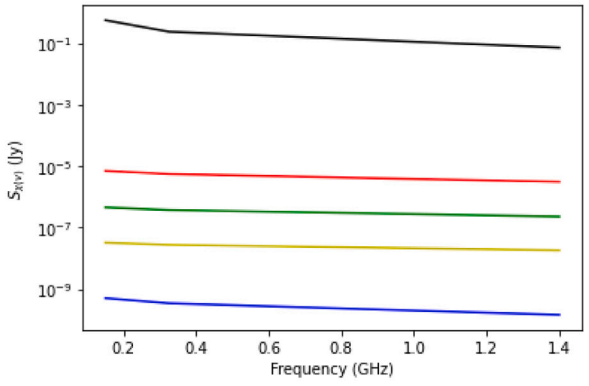


(d) DM particles candidates from SIMP: xd

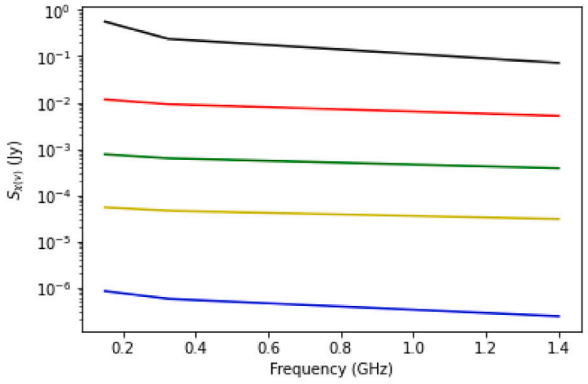


(e) DM particles candidates from SIMP: xr

**Fig. 4.** The DM annihilation emission in A1664 as calculated using Eq. (11). The black line represents the excess emission from Table 1. Four selected DM masses are shown (n1, a1, z1: 40 GeV in blue, 850 GeV in red, 1750 GeV in green, and 4000 GeV in yellow; xd, xr: 130 GeV in blue, 940 GeV in red, 1840 GeV in green, and 4000 GeV in yellow). The solid line represents the all annihilation channel (aac), the dashed line represents the $b\bar{b}$ channel, and the dash-dot line represents the $\mu^+\mu^-$ channel. Note that xr and xd only have aac. (For interpretation of the references to colour in this figure legend, the reader is referred to the web version of this article.)

## 3. Results and discussion

In the context of our analysis, the null hypothesis is defined as $S_{total} = S_{CR}$, while the DM hypothesis we are testing can be expressed as:

$$S_{total} = S_{CR} + S_{\chi} \tag{12}$$

Here, $S_{total}$ represents the total emission of the observed area as outlined in Table 1.

### 3.1. Cosmic ray data fitting

For our analysis, we utilized data acquired from [10]. We applied our in situ model, described by Eq. (4), to fit the radio relic data presented in Table 1 for both clusters, A4038 and A1664. The best-fitting parameters for A4038 and A1664 are depicted in Figs. 1 and 2, respectively. In our fitting process, we employed the "least-squared" method with error weighting based on the formula $1 + \frac{\text{error}}{\text{data}}$ to account for observational uncertainties.

A4038 continues to exhibit a strong fit with the observational data. However, it is important to note that our best-fitting parameters for A4038 differ from those reported in [7]. Despite this difference, the average deviation between Eq. (4) and the adiabatic compression model by [10] for A4038 is relatively small, measuring as low as 6% (see Fig. 1). While our analysis has demonstrated a relatively small average deviation of 6% between Eq. (4) and the adiabatic compression model for A4038, the adiabatic compression model may be over fitting the

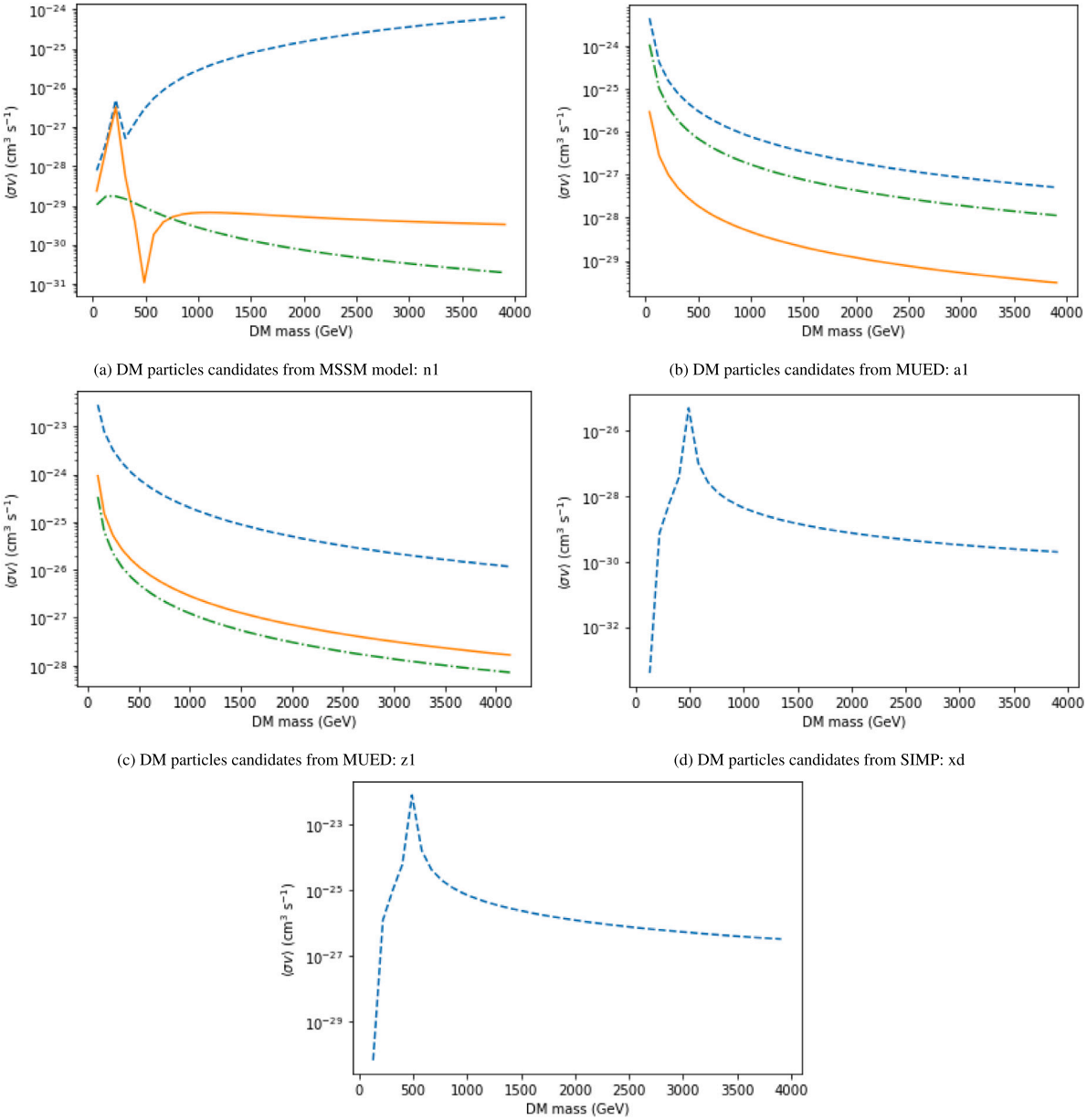


(a) DM particles candidates from MSSM model: n1

(b) DM particles candidates from MUED: a1

(c) DM particles candidates from MUED: z1

(d) DM particles candidates from SIMP: xd

(e) DM particles candidates from SIMP: xr

**Fig. 5.** The scaling between DM mass with $\langle \sigma v \rangle$ at 1.4 GHz. The blue dashed line represents aac. While orange solid and green dash-dot lines represent $b\bar{b}$ and $\mu^+\mu^-$ channels respectively. Note that xr and xd only have aac. (For interpretation of the references to colour in this figure legend, the reader is referred to the web version of this article.)

data. This implies that while the observed deviations may appear minimal, they could be influenced by the model's tendency to excessively adapt to the intricacies of the dataset, rather than reflecting genuine physical trends.

On the other hand, A1664 also maintains a good fit, although it shows a slightly higher value at 1.4 GHz compared to the observations. The average deviation for A1664 is approximately 20% (see Fig. 2). It is crucial to acknowledge that these deviations and differences in fitting parameters, especially for A1664, may introduce uncertainties in our results. The average deviation of 20% for A1664 raises concerns about the robustness of the fit.

Nonetheless, we maintain confidence that these differences and average deviations, while noteworthy, may not significantly impact our subsequent analysis. It is important to consider that these variations fall within the acceptable range of data error weights. However, readers should exercise caution in interpreting results, particularly for A1664.

### 3.2. DM annihilation emission

We fixed the DM mass for all five candidates within the range of 40 GeV to 4000 GeV. We specifically focused on three extreme fundamental annihilation channels: $b\bar{b}$, $\mu^+\mu^-$, and the all-annihilation channel (aac). Using the MadDM software, we computed the expected annihilation signals for all models, employing the calculations outlined in Section 2.4. Figs. 3 and 4 illustrate the DM annihilation emissions for A4038 and A1664, respectively.

The DM mass plays a critical role in determining the DM annihilation emission. Specifically, for the n1 candidate from MSSM, lower mass values result in lower emissions, while higher masses lead to increased emissions. However, this relationship primarily applies to the all-annihilation channel (aac). In contrast, for the $b\bar{b}$ and $\mu^+\mu^-$ channels, lower n1 mass values result in higher emissions, and vice versa. Fig. 5(a) showed a proportional scaling relationship between

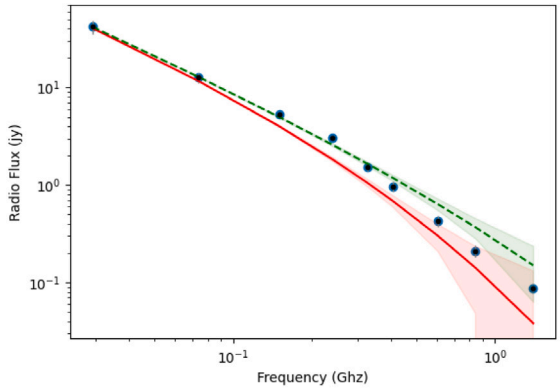


(a) DM particles candidates from MSSM model: n1

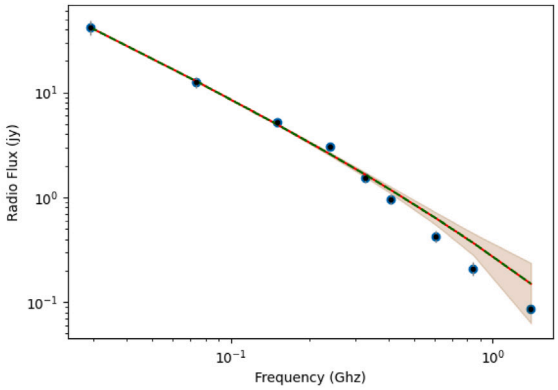


(b) DM particles candidates from MUED: a1

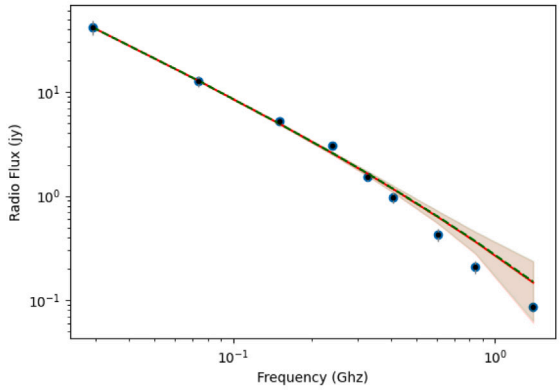


(c) DM particles candidates from MUED: z1

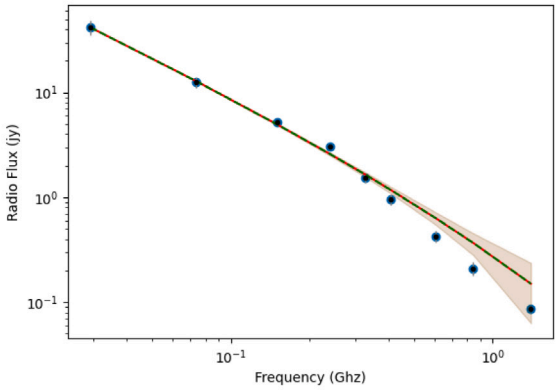


(d) DM particles candidates from SIMP: xd

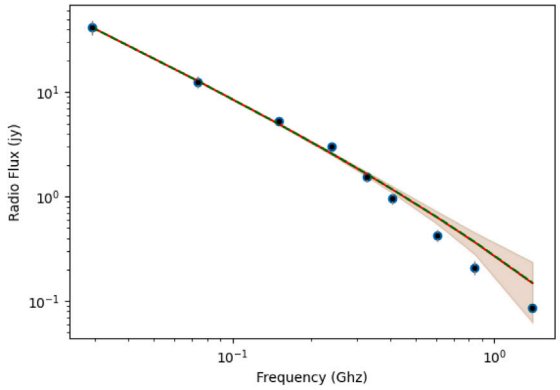


(e) DM particles candidates from SIMP: xr

**Fig. 6.** The plotted points are the total emission in A4038 from Table 1. The data are taken from [10]. The red solid line represents the DM hypothesis and the green dashed line represents the null hypothesis. The shaded region represents the 95% confidence level. (For interpretation of the references to colour in this figure legend, the reader is referred to the web version of this article.)

n1 mass with $\langle\sigma v\rangle$ for aac. While $\mu^+\mu^-$ and $b\bar{b}$ channels exhibit vice versa. However, at n1<500 GeV, the scaling of $\langle\sigma v\rangle$ had a fluctuating relationship with n1 mass for all three channels. This could be indicative of the likelihood of self-annihilation increasing at a higher n1 mass and fluctuating at n1<500 GeV. Potential contributors to these fluctuations may include resonance effects, threshold behaviour, or specific model features that manifest differently at lower n1 masses which is an interesting point for further study.

In the case of the a1 and z1 candidates from MUED, lower mass values produce higher emissions, and this pattern applies across all annihilation channels. In Fig. 5(b) and (c), the low mass values for a1 and z1 candidates exhibit the highest $\langle\sigma v\rangle$ across all annihilation channels. This consistent pattern implies a higher likelihood of self-annihilation at lower masses for a1 and z1 candidates, as indicated by the increased emissions observed. It is worth noting that emissions from lower mass values often exceed the total emissions of the observed area. Nevertheless, we still consider the low-mass scenarios in our analysis.

For the xd and xr candidates from SIMP, the emission seems to increase at a lower mass and then drop at a certain mass as the mass increases further. As shown in Fig. 5(d) and (e) the scaling of $\langle\sigma v\rangle$ has a peak at $\approx$ 490 GeV. This peak can be considered as a critical mass value where the emission spectrum peaks within the observed frequency range, contributing to the observed variations. Like n1, this

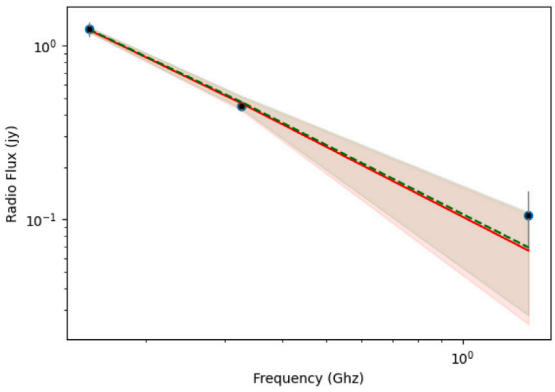


(a) DM particles candidates from MSSM model: n1

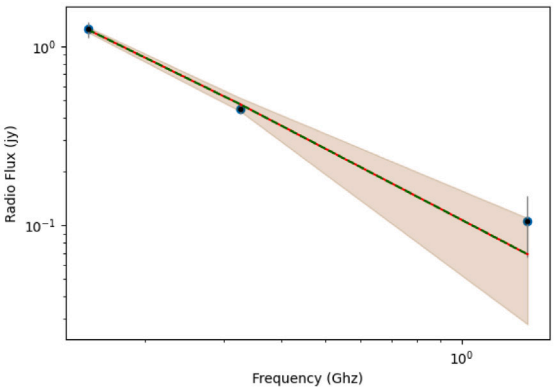


(b) DM particles candidates from MUED: a1

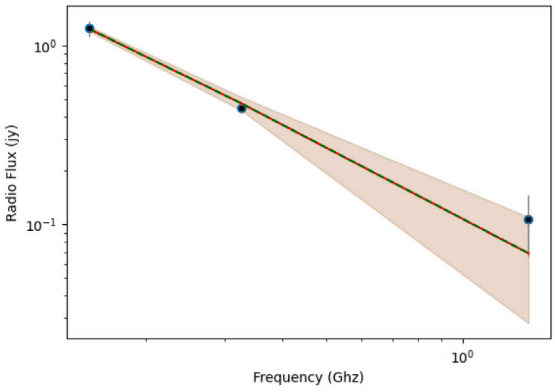


(c) DM particles candidates from MUED: z1

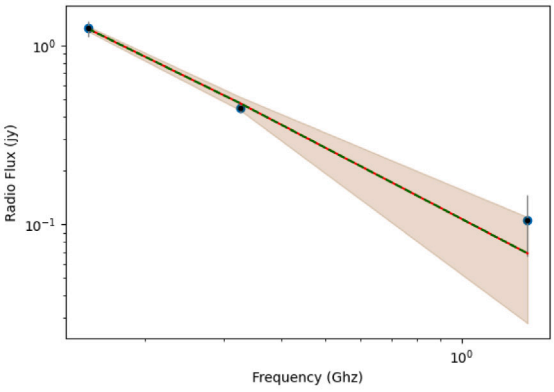


(d) DM particles candidates from SIMP: xd

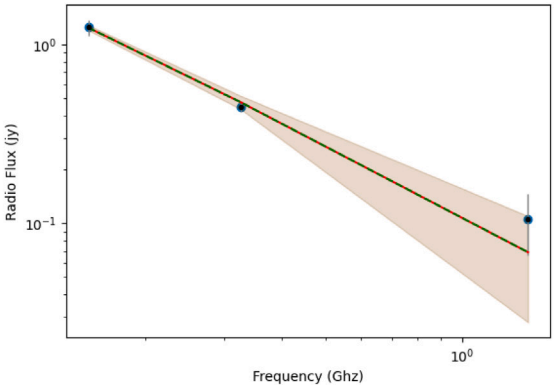


(e) DM particles candidates from SIMP: xr

**Fig. 7.** The plotted points are the total emission in A1664 from Table 1. The data are taken from [10]. The red solid line represents the DM hypothesis and the green dashed line represents the null hypothesis. The shaded region represents the 95% confidence level. (For interpretation of the references to colour in this figure legend, the reader is referred to the web version of this article.)

behaviour could be attributed to factors like resonance effects, threshold, or unique characteristics within the SIMP model that manifest differently at various DM masses which is also an interesting point for further study. Overall, A4038 exhibits higher emissions in comparison to A1664, which we attribute to A1664 having a lower DM number density relative to A4038.

We also generated plots illustrating the excess emission within the dark matter (DM) emission graph for A4038. In the case of the n1 mass category with masses greater than 850 GeV, the emissions from the aac channel exceed the excess emissions, while for a1, all three channels with masses less than 40 GeV surpass the excess emissions. As for z1, the aac channel with masses less than 1750 GeV and all three channels with masses less than 40 GeV are higher than the excess emissions. However, for xd, none of the mass values exceed the excess emissions, and for xr, only the mass of 940 GeV is higher than the excess emissions.

We then created similar plots for A1664, comparing the excess emissions with DM emissions. In A1664, no mass value in n1, xd, and xr exceeds the excess emissions. For a1, only two channels (aac and $\mu^+\mu^-$) with masses less than 40 GeV are higher than the excess emissions. In z1, all three channels with masses less than 40 GeV surpass the excess emissions.

These results do not provide sufficient clarity to conclusively establish that excess emissions originate from DM self-annihilation. We will proceed to the next section to further analyse the DM hypothesis.

**Table 4**
The emission of our DM particles and DM particle of [7] in A4038 at 1.4 GHz.

| Particle mass | Emission (Jy) | | | | | |
|---|---|---|---|---|---|---|
| | n1 | a1 | z1 | xd | xr | [7] |
| 130 GeV | 0.012 | 0.19 | 0.22 | 1.44e−08 | 2.39e−05 | 0.3-0.4 |

### 3.3. DM hypothesis analysis

We employed the same statistical analysis method as outlined in [7] to assess the validity of our DM hypothesis. The test statistic (TS) used in our analysis can be described by the formula:

$$TS = -2\ln\left(\frac{L_0}{L}\right) \tag{13}$$

In this equation, $L_0$ represents the likelihood of the null hypothesis, while $L$ is the likelihood of the DM hypothesis. Both likelihood values can be computed using the following equation:

$$L_0; L \propto \exp(-\chi^2) \tag{14}$$

Here, $\chi$ corresponds to the chi-squared values.

Figs. 6 and 7 depict the fitting of our hypotheses for the total emission of the observed area in both clusters.

However, it is noteworthy that our test statistic (TS) values for all DM masses and channels, across all particle candidates, resulted in negative values in the A4038 cluster. Negative TS values are indeed unusual, but in the context of our one-sided DM hypothesis, they are acceptable. Nevertheless, we believe that these TS values lack sufficient evidence to warrant the rejection of our null hypothesis. In contrast to the findings of [7], we did not find the DM hypothesis acceptable for the A4038 cluster.

Our assumptions for the A4038 cluster are supported by the results obtained for the A1664 cluster. In A1664, the TS values for all DM masses and channels, across all particle candidates, are less than 1. Our null hypothesis is accepted here. This reinforces our belief that Eq. (4) is not suitable for clusters other than A4038.

It is crucial to acknowledge that the inclusion of DM particles in our DM hypothesis is the primary reason our assumptions were rejected in both clusters. It is noteworthy that in their work, [7] utilized the hydrostatic equilibrium (HE) profile to calculate DM density in A4038. Fig. 8 illustrates that the HE profile exhibits higher density in comparison to the NFW profile. Moreover, [36] found that the HE profile had an average deviation of about 10%–20% out to the virial radius. The selection of the NFW profile for the study of DM particles in galaxy clusters is consistent with other research conducted by [37,38].

The emissions of DM particles across all models at the same mass as in [7] exhibit lower values. This suggests that the DM hypothesis ($S_{CR} + S_\chi$) cannot fit as well as demonstrated in [7]. Table 4 displays the emissions of n1, a1, z1, xd, and xr, compared to the DM emission obtained in [7] at 130 GeV for the $b\bar{b}$ channel in A4038 at 1.4 GHz. It is essential to note that [7] took into account the substructures in galaxy clusters by incorporating the boost factor [39], which can enhance the annihilation rate.

The application of Eq. (4) in the case of A1664 may be considered inadequate, primarily due to the limited number of available data points. Despite this limitation, our results indicate that Eq. (4) exhibits a satisfactory fit with the adiabatic compression model, particularly at low frequencies. It is important to underscore, however, that the reliability and robustness of the fitted parameters for A1664 are compromised by the scarcity of data points.

The limited data points for A1664 pose challenges in accurately constraining the parameters of Eq. (4), and as such, the results should be interpreted with caution. We acknowledge the necessity for more data in A1664 to produce results with increased robustness.

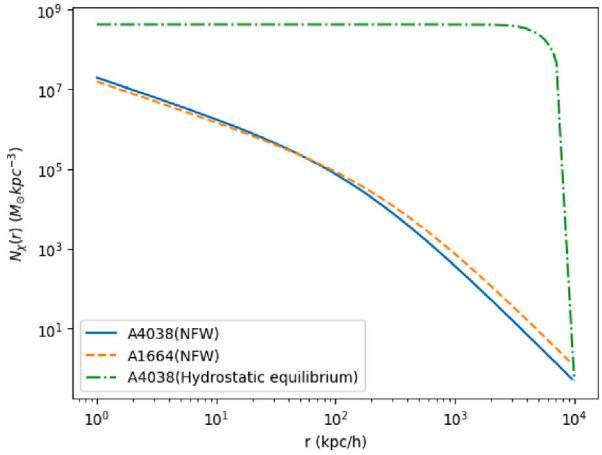


**Fig. 8.** DM density profile in A4038 and A1664. The green dash-dot line is DM density profile using hydrostatic equilibrium [7]. (For interpretation of the references to colour in this figure legend, the reader is referred to the web version of this article.)

### 3.4. DM cross-section annihilation upper limit

We adopted the same methodology as outlined in [38] to determine the upper limit on the DM cross-section annihilation. The relationship between $S_\chi$, $\langle\sigma v\rangle$, and $m_\chi$ can be expressed as follows:

$$log\left(\frac{S_\chi}{\langle\sigma v\rangle}\right) = c_1 log(m_\chi + c_2) + c_3 \tag{15}$$

Here, $S_\chi$ was derived from Eq. (11), while $\langle\sigma v\rangle$ and $m_\chi$ were obtained using MadDM software [23]. Utilizing this relationship, we can calculate the upper limit on $\langle\sigma v\rangle$ as follows:

$$\langle\sigma v\rangle \leq 10^{logS_\chi - c_1 log(m_\chi + c_2) + c_3} \tag{16}$$

Here, $S_\chi$ represents the total emission of the observed area as outlined in Table 1. Figs. 9 and 10 illustrate the upper limit on $\langle\sigma v\rangle$ obtained from Eq. (16) for A4038 and A1664, respectively.

In A4038, our upper limit is nearly identical to that of [37,38], with the n1 particle from the MSSM model having the highest upper limit, reaching approximately 0.029 GHz. A similar trend was observed in A1664, with a slightly higher upper limit, and the a1 particle from the MUED model exhibited the highest upper limit at 0.15 GHz. When averaging the upper limit values, our results indicate a more stringent upper limit in comparison to the previous study by [37,38]. Notably, the $b\bar{b}$ and $\mu^+\mu^-$ channels yielded upper limits on $\langle\sigma v\rangle$ that are nearly equivalent to those of the all-annihilation channel (aac). Consequently, we chose not to present both upper limit channels in Figs. 8 and 9.

## 4. Conclusion

In this study, we investigated three models beyond the Standard Model (SM) featuring five particles as candidates for DM. Our analysis revealed that these DM particle candidates conform to the NFW profile distribution in both the A4038 and A1664 galaxy clusters. This assumption is supported by studies such as [37,38] that have used the NFW profile in similar astrophysical environments. We estimated the synchrotron emission ($S_\chi$) from the annihilation products of these DM candidates, accounting for the influence of intracluster magnetic fields. Our work focused on understanding the excess emission based on radio observations.

The observational uncertainties for both A4038 and A1664 were found to be minimal (as referred to in [10]). These reduced uncertainties allowed us to identify strong signals that we attribute to DM annihilation. Notably, one of the sources of uncertainty in identifying radio signals from DM annihilation is the magnetic properties of the

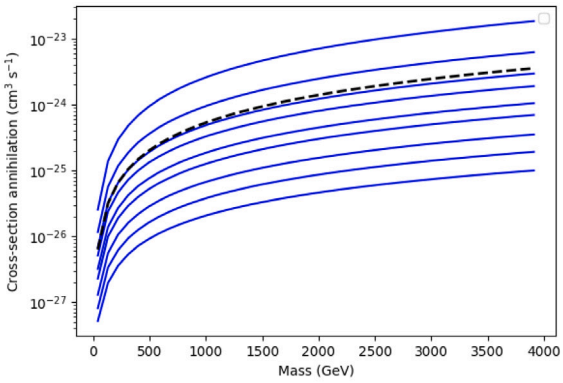


(a) DM particles candidates from MSSM model: n1

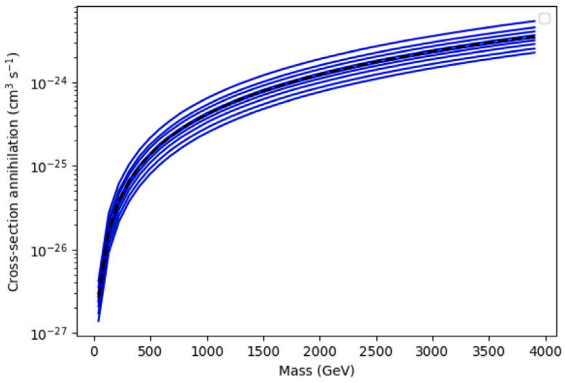


(b) DM particles candidates from MUED: a1

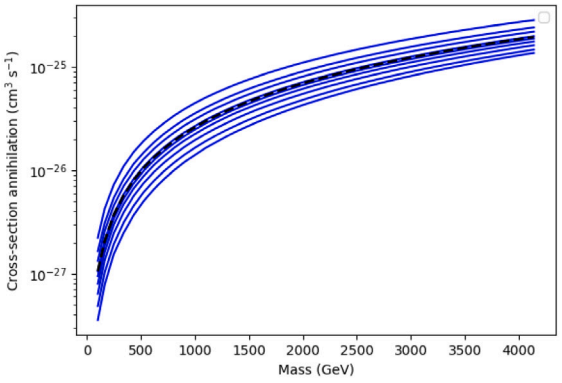


(c) DM particles candidates from MUED: z1

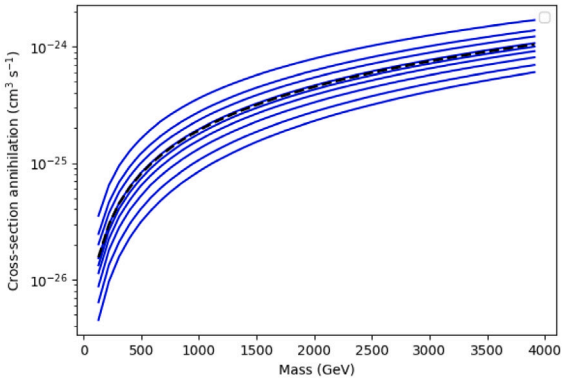


(d) DM particles candidates from SIMP: xd

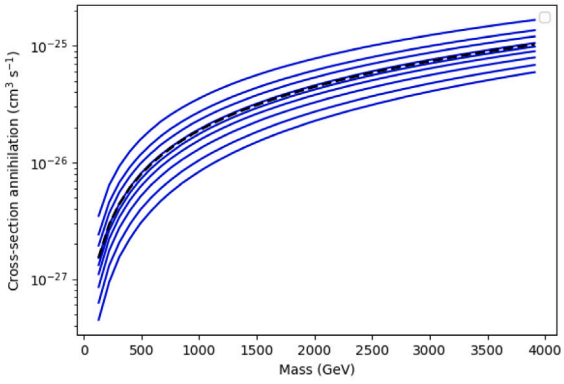


(e) DM particles candidates from SIMP: xr

**Fig. 9.** The upper limit on $\langle \sigma v \rangle$ is obtained from Eq. (16) in A4038. The solid line shows the upper limit on $\langle \sigma v \rangle$ for the different frequencies with the highest upper limit for the lowest frequency (0.029 GHz) and the lowest upper limit for the highest frequency (1.4 GHz). Note that all DM particle candidates presented are under the same conditions. The dashed line represents the average of the upper limit on $\langle \sigma v \rangle$ in A4038.

clusters, such as $B_0$, $\eta$, $\beta$, and $n_{gas}$. However, the impact of these uncertainties was deemed insignificant, as previously reported in [37,38], and [7].

We acknowledge that Eq. (4) may be oversimplified and primarily suited for A4038, given its elongated relic structure, as opposed to the circular relic observed in A1664. We speculate that with more precise calculations or simulations, it might be possible to obtain the test statistic (TS) value supporting the DM hypothesis, akin to the findings in [7]. Furthermore, Eq. (11) does not consider the substructure of the clusters in its calculation or simulation. We anticipate that incorporating substructures could enhance DM emission. Nevertheless, as Eq. (11) assumes a spherically symmetric cluster shape, our DM emission can be considered an upper limit of the radio signal for DM annihilation.

The limited data points of A1664 also affected the application of Eq. (4). However, it is crucial to recognize the impact of the data limitation on the reliability of our results. Future research endeavours should prioritize the acquisition of additional data for A1664 to strengthen the robustness of our models. Additional observational data will not only enhance the accuracy of parameter estimation but also contribute to a more comprehensive understanding of the DM emission in A1664.

The presence of discrete sources significantly affects the assessment of excess emissions in our study. While both selected clusters have discrete sources, problems may arise if the excess emission does not correspond to the existence of discrete sources. Other studies have

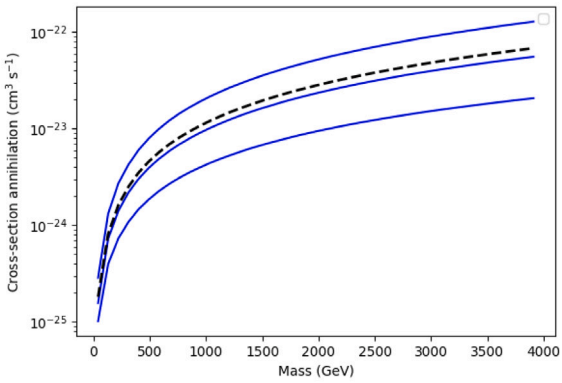


(a) DM particles candidates from MSSM model: n1

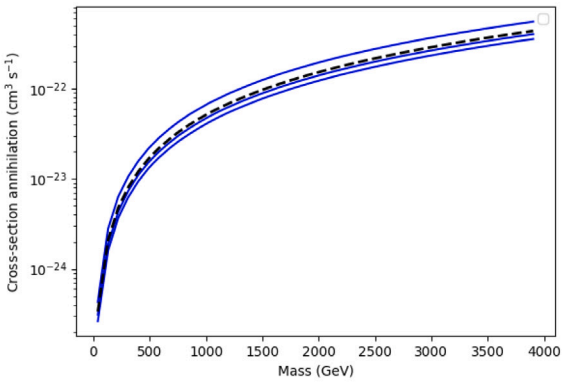


(b) DM particles candidates from MUED: a1

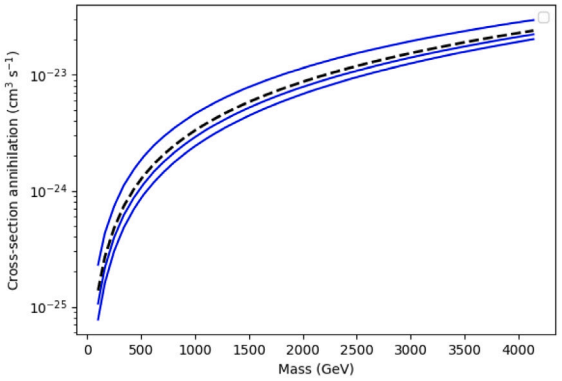


(c) DM particles candidates from MUED: z1

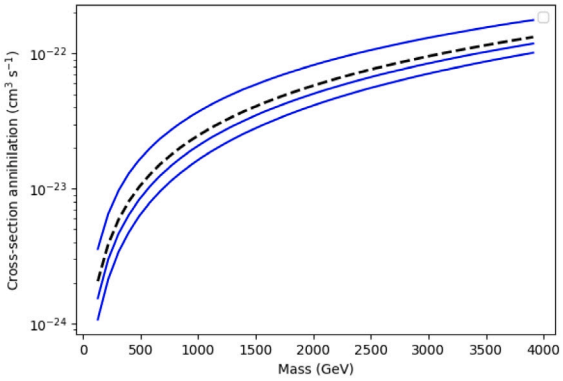


(d) DM particles candidates from SIMP: xd

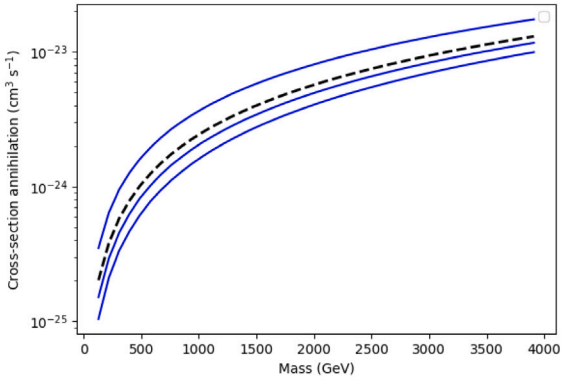


(e) DM particles candidates from SIMP: xr

**Fig. 10.** The upper limit on $\langle \sigma v \rangle$ is obtained from Eq. (16) in A1664. The solid line shows the upper limit on $\langle \sigma v \rangle$ for the different frequencies with the highest upper limit for the lowest frequency (0.15 GHz) and the lowest upper limit for the highest frequency (1.4 GHz). Note that all DM particle candidates presented are under the same conditions. The dashed line represents the average of the upper limit on $\langle \sigma v \rangle$ in A1664.

attempted to explain excess emissions as originating from cluster mergers [8] and secondary ultra-relativistic electrons [9]. However, these explanations still require further investigation and observation. Assuming that excess emission arises from the subtraction of the total emission of the observation area with radio relics and/or radio halo emissions, additional studies and samples of galaxy clusters are essential to refine the definition of excess emissions and account for the observations in A4038 and A1664.

Another interpretation of excess emission can be attributed to standard astrophysical processes, including the diffuse gamma-ray background, the injection of cosmic rays at the galactic centre, or unresolved point sources such as young pulsars or millisecond pulsars (MSPs) [40]. This alternative perspective is valuable for identifying each source of excess emission, allowing us to establish a more robust definition for excess emission.

Despite the negligible excess emission coming from DM, we maintain the belief that DM does impact the radio continuum spectral data of galaxy clusters. Considering that our total emission of the observation area in this paper pertains only to the peripheral regions of clusters, we recognize the potential for detecting DM emissions in other regions.

In conclusion, our study underscores the value of fitting analysis to radio data observations as an effective means of detecting DM particles. While acknowledging the limitations and uncertainties, we successfully established the upper limit of $\langle \sigma v \rangle$ in A4038 and A1664. These upper limits of $\langle \sigma v \rangle$ will improve the DM candidates for the refinement of excess emission definition.

## CRediT authorship contribution statement

**Z.Z. Abidin:** Writing – original draft, Validation, Supervision, Project administration, Methodology, Funding acquisition, Conceptualization. **N. Asmi:** Writing – review & editing, Investigation, Formal analysis, Data curation, Conceptualization. **M.R. Mat Sabri:** Writing – original draft, Visualization, Validation, Supervision, Methodology, Formal analysis, Data curation, Conceptualization. **M.A. Rohaizi:** Resources, Investigation, Conceptualization. **N. Hashim:** Validation, Formal analysis, Data curation. **U.F.S.U. Ibrahim:** Writing – review & editing, Validation, Conceptualization.

## Declaration of competing interest

The authors declare that they have no known competing financial interests or personal relationships that could have appeared to influence the work reported in this paper.

## Data availability

Data will be made available on request.

## Acknowledgements

This research is supported by the University Malaya's Faculty of Science Grant, GPF081-2020 and GPF003H-2019.

## References

[1] N. Aghanim, Y. Akrami, M. Ashdown, J. Aumont, C. Baccigalupi, M. Ballardini, A. Banday, R. Barreiro, N. Bartolo, S. Basak, et al., Erratum: Planck 2018 results: VI. Cosmological parameters, Astron. Astrophys. 641 (2020) A6(2021).

[2] P. Natarajan, D. Croton, G. Bertone, Consequences of dark matter self-annihilation for galaxy formation, Mon. Not. R. Astron. Soc. 388 (4) (2008) 1652–1666, http://dx.doi.org/10.1111/j.1365-2966.2008.13306.x, arXiv:https://academic.oup.com/mnras/article-pdf/388/4/1652/3038625/mnras0388-1652.pdf.

[3] E. Storm, T.E. Jeltema, M. Splettstoesser, S. Profumo, Synchrotron emission from dark matter annihilation: Predictions for constraints from non-detections of galaxy clusters with new radio surveys, Astrophys. J. 839 (1) (2017) 33, http://dx.doi.org/10.3847/1538-4357/aa6748.

[4] E. Storm, T. Jeltema, M. Splettstoesser, S. Profumo, Synchrotron emission from dark matter annihilation: Predictions for constraints from non-detections of galaxy clusters with new radio surveys, Astrophys. J. 839 (2016) http://dx.doi.org/10.3847/1538-4357/aa6748.

[5] A. McDaniel, T. Jeltema, S. Profumo, A multi-wavelength analysis of annihilating dark matter as the origin of the Gamma-ray emission from M31, Phys. Rev. D 97 (2018) http://dx.doi.org/10.1103/PhysRevD.97.103021.

[6] F. Loi, F. Govoni, M. Murgia, V. Vacca, H. Li, L. Feretti, G. Giovannini, Magnetic fields in galaxy clusters in the SKA era, J. Phys. Conf. Ser. 841 (2017) 012005, http://dx.doi.org/10.1088/1742-6596/841/1/012005.

[7] M.H. Chan, C.M. Lee, An excess radio signal in the Abell 4038 cluster, Mon. Not. R. Astron. Soc. 500 (4) (2020) 5583–5588, http://dx.doi.org/10.1093/mnras/staa2895, arXiv:https://academic.oup.com/mnras/article-pdf/500/4/5583/34925825/staa2895.pdf.

[8] K. Fang, T. Linden, Cluster mergers and the origin of the ARCADE-2 excess, J. Cosmol. Astropart. Phys. 2016 (10) (2016) 004, http://dx.doi.org/10.1088/1475-7516/2016/10/004.

[9] A.N. Timokhin, F.A. Aharonian, A.Y. Neronov, On the non-thermal high energy radiation of galaxy clusters, Astron. Astrophys. 417 (2) (2004) 391–399, http://dx.doi.org/10.1051/0004-6361:20040004.

[10] R. Kale, K.S. Dwarakanath, Multi-frequency studies of radio relics in the galaxy clusters A4038, A1664, AND A786, Astrophys. J. 744 (1) (2011) 46, http://dx.doi.org/10.1088/0004-637x/744/1/46.

[11] O. Slee, A. Roy, M. Murgia, H. Andernach, M. Ehle, Four extreme relic radio sources in clusters of galaxies, Astron. J. 122 (3) (2001) 1172.

[12] J.F. Navarro, C.S. Frenk, S.D.M. White, A universal density profile from hierarchical clustering, Astrophys. J. 490 (2) (1997) 493–508, http://dx.doi.org/10.1086/304888, arXiv:astro-ph/9611107.

[13] A.M. Groener, D.M. Goldberg, M. Sereno, The galaxy cluster concentration–mass scaling relation, Mon. Not. R. Astron. Soc. 455 (1) (2016) 892–919.

[14] B. Diemer, COLOSSUS: A python toolkit for cosmology, large-scale structure, and dark matter halos, Astrophys. J. Suppl. Ser. 239 (2) (2018) 35.

[15] F. Govoni, L. Feretti, Magnetic fields in clusters of galaxies, Internat. J. Modern Phys. D 13 (08) (2004) 1549–1594.

[16] Y. Chen, T. Reiprich, H. Böhringer, Y. Ikebe, Y.-Y. Zhang, Statistics of X-ray observables for the cooling-core and non-cooling core galaxy clusters, Astron. Astrophys. 466 (3) (2007) 805–812.

[17] K. Dolag, S. Schindler, F. Govoni, L. Feretti, Correlation of the magnetic field and the intra-cluster gas density in galaxy clusters, Astron. Astrophys. 378 (3) (2001) 777–786.

[18] F. Govoni, L. Feretti, G. Giovannini, H. Böhringer, T. Reiprich, M. Murgia, Radio and X-ray diffuse emission in six clusters of galaxies, Astron. Astrophys. 376 (3) (2001) 803–819.

[19] W. Jaffe, Origin and transport of electrons in the halo radio source in the coma cluster, Astrophys. J. 212 (1977) 1–7.

[20] J. Roland, On the origin of the intergalactic magnetic field and of the radio halo associated with the coma cluster of galaxies, Astron. Astrophys. 93 (1981) 407–410.

[21] R. Schlickeiser, A. Sievers, H. Thiemann, The diffuse radio emission from the Coma cluster, Astron. Astrophys. 182 (1987) 21–35.

[22] M. Thierbach, U. Klein, R. Wielebinski, The diffuse radio emission from the Coma cluster at 2.675 GHz and 4.85 GHz, Astron. Astrophys. 397 (1) (2003) 53–61.

[23] F. Ambrogi, C. Arina, M. Backović, J. Heisig, F. Maltoni, L. Mantani, O. Mattelaer, G. Mohlabeng, MadDM v.3.0: A comprehensive tool for dark matter studies, Phys. Dark Universe 24 (2019) 100249, http://dx.doi.org/10.1016/j.dark.2018.11.009.

[24] A. Alloul, N.D. Christensen, C. Degrande, C. Duhr, B. Fuks, FeynRules 2.0 — A complete toolbox for tree-level phenomenology, Comput. Phys. Comm. 185 (8) (2014) 2250–2300, http://dx.doi.org/10.1016/j.cpc.2014.04.012.

[25] H. Nilles, Supersymmetry, supergravity and particle physics, Phys. Rep. 110 (1) (1984) 1–162, http://dx.doi.org/10.1016/0370-1573(84)90008-5, URL https://www.sciencedirect.com/science/article/pii/0370157384900085.

[26] H. Haber, G. Kane, The search for supersymmetry: Probing physics beyond the standard model, Phys. Rep. 117 (2) (1985) 75–263, http://dx.doi.org/10.1016/0370-1573(85)90051-1, URL https://www.sciencedirect.com/science/article/pii/0370157385900511.

[27] H.-C. Cheng, K.T. Matchev, M. Schmaltz, Bosonic supersymmetry? Getting fooled at the CERN LHC, Phys. Rev. D 66 (5) (2002) http://dx.doi.org/10.1103/physrevd.66.056006.

[28] H.-C. Cheng, K.T. Matchev, M. Schmaltz, Radiative corrections to kaluza-klein masses, Phys. Rev. D 66 (3) (2002) http://dx.doi.org/10.1103/physrevd.66.036005.

[29] M. Backović, M. Krämer, F. Maltoni, A. Martini, K. Mawatari, M. Pellen, Higher-order QCD predictions for dark matter production at the LHC in simplified models with s-channel mediators, 2015, http://dx.doi.org/10.48550/ARXIV.1508.05327, URL https://arxiv.org/abs/1508.05327.

[30] A. Albert, M. Backovic, A. Boveia, O. Buchmueller, G. Busoni, A. De Roeck, C. Doglioni, T. DuPree, M. Fairbairn, M.-H. Genest, S. Gori, G. Gustavino, K. Hahn, U. Haisch, P.C. Harris, D. Hayden, V. Ippolito, I. John, F. Kahlhoefer, S. Kulkarni, G. Landsberg, S. Lowette, K. Mawatari, A. Riotto, W. Shepherd, T.M.P. Tait, E. Tolley, P. Tunney, B. Zaldivar, M. Zinser, Recommendations of the LHC dark matter working group: Comparing lhc searches for heavy mediators of dark matter production in visible and invisible decay channels, 2017, http://dx.doi.org/10.48550/ARXIV.1703.05703, URL https://arxiv.org/abs/1703.05703.

[31] P.C. Tribble, Radio spectral ageing in a random magnetic field, Mon. Not. R. Astron. Soc. 261 (1) (1993) 57–62.

[32] S.T. Myers, S.R. Spangler, Synchrotron aging in the lobes of luminous radio galaxies, Astrophys. J Part 1 (ISSN: 0004-637X) 291 (1985) 52–62.

[33] C. Carilli, R. Perley, J. Dreher, J. Leahy, Multifrequency radio observations of cygnus A-spectral aging in powerful radio galaxies, Astrophys. J. 383 (1991) 554–573.

[34] C.L. Sarazin, The energy spectrum of primary cosmic-ray electrons in clusters of galaxies and inverse compton emission, Astrophys. J. 520 (2) (1999) 529–547, http://dx.doi.org/10.1086/307501.

[35] G. Ghisellini, P.W. Guilbert, R. Svensson, The synchrotron boiler, Astrophys. J. Lett. 334 (1988) L5, http://dx.doi.org/10.1086/185300.

[36] V. Biffi, S. Borgani, G. Murante, E. Rasia, S. Planelles, G.L. Granato, C. Ragone-Figueroa, A.M. Beck, M. Gaspari, K. Dolag, On the nature of hydrostatic equilibrium in galaxy clusters, Astrophys. J. 827 (2) (2016) 112.

[37] E. Storm, T.E. Jeltema, S. Profumo, L. Rudnick, Constraints on dark matter annihilation in clusters of galaxies from diffuse radio emission, Astrophys. J. 768 (2) (2013) 106.

[38] C.-Y. Kiew, C.-Y. Hwang, Z. Zainal Abibin, Constraints on the dark matter neutralinos from the radio emissions of galaxy clusters, Mon. Not. R. Astron. Soc. 467 (3) (2017) 2924–2933, http://dx.doi.org/10.1093/mnras/stx288, arXiv:https://academic.oup.com/mnras/article-pdf/467/3/2924/10875770/stx288.pdf.

[39] M.A. Sánchez-Conde, F. Prada, The flattening of the concentration–mass relation towards low halo masses and its implications for the annihilation signal boost, Mon. Not. R. Astron. Soc. 442 (3) (2014) 2271–2277.

[40] S.K. Lee, M. Lisanti, B.R. Safdi, Distinguishing dark matter from unresolved point sources in the inner galaxy with photon statistics, J. Cosmol. Astropart. Phys. 2015 (05) (2015) 056.